RAL–TR–1999–018
February 1999

The phenomenology of top quark polarisation in the decay of heavy charged Higgs bosons at LHC and beyond

Kosuke Odagiri

Rutherford Appleton Laboratory,
Chilton, Didcot, Oxon OX11 0QX, UK.

Abstract

It has recently been shown that through the $\tau\nu$ decay mode the heavy charged Higgs bosons $H^{\pm}$ can be discovered at LHC over a vast region of the parameter space previously thought unaccessible. If the charged Higgs bosons are discovered in this decay mode and the measurements of its mass and $\tan\beta$ are made, it allows us to make greater use of the dominant but QCD background contaminated bt decay mode by cuts suppressing phase space for the background. In this paper we study the top quark polarisation in the bt decay mode. When $\tan\beta$ is either moderately large ($\tan\beta \gtrsim 9$) or small ($\tan\beta \lesssim 4$), the correlation effects can be used as a signal of $H^{\pm}$ production. We outline the analysis procedure for various decay signatures. As an example, we demonstrate the application of our procedure to the dominant production process $gb \to tH^{-}$ at LHC. The effect is clearly observable for $H^{\pm}$ mass between 200 GeV and 500 GeV in both leptonic and hadronic channels, but at 500 GeV the boost on the top quark starts to prevent the reconstruction of invariant masses, and hence the observation of the correlation effect, in the hadronic decay channel.

1 Introduction

The charged Higgs bosons $H^\pm$ are a central ingredient of the Two Higgs Doublet Model (2HDM) which is not only an attractive alternative to the Standard Model single Higgs doublet but is also inherent in the supersymmetric models, notably Minimal Supersymmetric Standard Model (MSSM). Within the framework of MSSM, recent experimental analyses [1, 2] point to the heavy ($M_{H^\pm} \gtrsim m_t$) mass region, where they can not be produced in top quark decay, and their dominant decay $H^\pm \to bt$ suffers from large QCD background.

In [3] the author has shown that the $\tau\nu$ decay mode of the heavy charged Higgs bosons $H^\pm$ offers a striking signature of high p_T tau and large missing energy through which $H^\pm$ can be discovered readily at LHC, provided that the top quark momentum in the dominant production process $gb \to tH^-$ is constrained. Although the signal cross section falls markedly at large $M_{H^\pm}$ and small $\tan\beta$, it was claimed that for $\tan\beta \gtrsim 3$ and $M_{H^\pm} \lesssim 1$ TeV the signal is sizeable enough after selection cuts to compete with the irreducible background and the finite LHC luminosity.

Given now that heavy $H^\pm$ can be discovered in the $\tau\nu$ decay mode for much of the parameter space, and that $M_{H^\pm}$ and $\tan\beta$ can be measured to certain extent using the tau and missing transverse momenta distributions and the total cross section, it is desirable to be able to narrow down the parameters further by utilising the dominant decay mode bt.

The bt decay mode of $H^\pm$, following production from the parton level process $gb \to tH^-$, has been studied extensively in the literature [4] from the viewpoint of the search for heavy $H^\pm$. The utility of the bt decay mode is limited for this purpose because of the contamination from QCD background. However, given that $M_{H^\pm}$ and $\tan\beta$ can be measured in the $\tau\nu$ decay mode, this can be used to constrain the final state.

In this paper we study the effect of top quark polarisation from $H^\pm$ decay on parton level observables, noting that the top quark is polarised by the chiral coupling of $H^\pm$ to bt, for either large or small $\tan\beta$. To be more precise, the two chiral components of the $H^\pm$ coupling to bt are proportional to $m_b \tan\beta$ and $m_t \cot\beta$ and the two balance out when $\tan\beta = \sqrt{m_t/m_b} \sim 6.4$ ($m_b = 4.25$ GeV). Far away from this central value, $\tan^4\beta \ll m_t^2/m_b^2$ or $\tan^4\beta \gg m_t^2/m_b^2$, the couplings are dominantly left or right leading to characteristic correlation patterns.

Our discussions are applicable to any class of production processes, but as an example for studying the effect of boosts on $H^\pm$ momenta we adopt the $gb \to tH^-$ production process at LHC.

When $\tan\beta \sim m_t/m_b$, the production cross section in the $gb \to tH^-$ reaches the minimum, while the correlation pattern will resemble the background, and our analysis will not be of much use. If the background reduction is almost perfect before the polarisation analysis, the polarisation measurement can be used to measure $\tan\beta$ accurately. This is presumably unlikely.

The use of right-handed tau polarisation as a characteristic signal of $H^\pm$ decay was studied in [5]. In addition, we note that if the tau is produced in the decay of the top quark through $H^\pm$, the distribution of invariant mass squared $M^2_{[b\tau]}$ is flat since there is no momentum correlation between the b from the decay of the top quark and the τ. This does not apply to the background from $W^\pm$ decay, and if we know the exact distribution, we can use it to measure the signal to background ratio and thus confirm

the tau polarisation analysis.

Our current work is in a similar vein. As in [5], the technique is not expected to be of great use in reducing the background, but once an excess of signal over background is observed near $H^\pm$ mass, the momentum correlations resulting from top quark polarisations can be used as a check for the signal presence in the sample and its proportion to the background.

We outline the analysis procedure for various decay signatures.

Finally, we note that a preliminary study of the top quark polarisation in $H^\pm$ decay was presented in [6]. Our present analysis is different in several ways. Firstly, the primary purpose of [6] is in measuring $\tan\beta$, rather than in distinguishing the signal from the background. Thus their analysis is applicable in a range of $\tan\beta$ complementary to the range emphasised here. Secondly, the variable utilised in [6], namely the leptonic energy in the $H^\pm$ rest frame, is not well defined unless $H^\pm$ is produced at an e^+e^- collider and decays leptonically with no other source of missing energy. In any case, for the intermediate region of $\tan\beta$ the production rate at hadronic colliders is small.

2 Calculation

We adopt $M_{H^\pm}$ and $\tan\beta$ as the two Higgs sector parameters. When calculating the width of $H^\pm$ in order to simulate the finite width effect, we assume that the bt branching ratio is 100%. The top branching ratio to $bW^\pm$ is also taken to be 100%, and $W^\pm$ branching ratio to a pair of fermions ff' is divided into quarks and leptons by the tree level ratios of 1/3 for each quark pair and 1/9 for each lepton pair. Note that unlike in reference [3], 'lepton', ℓ, always includes tau.

We restrict our discussions to the tree level. The dominant part of the radiative corrections [7], which are known to be significant, can be absorbed in terms of the running mass of the bottom quark and therefore does not affect the shapes of our distributions. We simulate the jet showering by imposing cuts between parton directions for the case of the hadronic decay of the top quark.

For simplicity we take the top quark mass to be 175 GeV for both Yukawa coupling and the kinematics, and the bottom quark mass to be 4.25 GeV, again for both Yukawa coupling and the kinematics. The fermions from $W^\pm$ decay are considered massless.

The electroweak parameters are $\alpha_{\rm EM} = 1/128$, $\sin^2\theta_W = 0.2315$, $M_Z = 91.187$ GeV, $M_W = M_Z\cos\theta_W \approx 79.94$ GeV. The Cabbibo–Kobayashi–Maskawa matrix element $V^2_{\rm CKM}[bt]$ is taken to be 1.

The tree level matrix elements squared are simple and are calculated by hand. Consistency checks are carried out between different limits. The numerical integrations are carried out using `VEGAS` [8] and the total decay width, in the narrow width limit of the propagators, agrees with the width calculated by hand.

3 Analysis

The decay matrix element squared, corresponding to the Feynman graph of figure 1, is given by:

$$\overline{|\mathcal{M}|^2} \;=\; 4N_C\left(\frac{e^2}{2\sin^2\theta_W}\right)^3 |\mathcal{G}_t\mathcal{G}_{W^\pm}|^2(2p_b\cdot p_\nu)(2p_t\cdot p_\ell)\times$$

$$\times \left[\left[g_b^2 (M_{H^\pm}^2 - m_b^2 - p_t^2) - 2 g_b g_t m_b m_t \right] + \frac{2 p_{\bar{b}} \cdot p_\ell}{2 p_t \cdot p_\ell} (g_t^2 m_t^2 - g_b^2 p_t^2) \right]. \quad (1)$$

We have defined $g_t = (m_t \cot\beta / M_W)$ and $g_b = (m_b \tan\beta / M_W)$. $\mathcal{G}_t$ and $\mathcal{G}_{W^\pm}$ are Breit-Wigner propagators for the top quark and W^+, respectively. In our analysis we also generate the $H^\pm$ mass with a Breit-Wigner distribution. This formula essentially carries all the information about momentum correlations. The effect of top quark polarisation is manifested in the second term in large square brackets which is proportional to $(2p_{\bar{b}} \cdot p_\ell)$. If the two chiral couplings were equal, the term vanishes in the limit of on-shell top quark.

In the limit of on-shell top quark and W^+ boson, the matrix element squared, and hence the differential decay rate, depend only on two independent dot products (or invariant masses), which we can take to be $(2p_{\bar{b}} \cdot p_\ell)$ and $(2p_b \cdot p_\ell)$ since these two quantities are measurable, as invariant masses, in the leptonic decay of the top quark, if bottom quark charge tagging is available. We have:

$$\begin{aligned} 2p_b \cdot p_\nu &= m_t^2 - m_b^2 - M_{W^\pm}^2 - 2p_b \cdot p_\ell \\ 2p_t \cdot p_\ell &= M_{W^\pm}^2 + 2p_b \cdot p_\ell \end{aligned} \quad (2)$$

and hence the above statement holds. Furthermore, from equations (1) and (2) we see that in the limit of non-chiral coupling, the dependence on $(2p_{\bar{b}} \cdot p_\ell)$ vanishes altogether, as would a general non-chiral background. Hence the dependence of the differential decay rate on $(2p_{\bar{b}} \cdot p_\ell)$ would be an indication of the presence of $H^\pm$. This would not hold if the two coupling strengths were similar, $g_t^2 \sim g_b^2$. This implies $\tan^4\beta \sim m_t^2/m_b^2$.

In experimental analyses, a possible approach would be to fit the multi-dimensional differential decay distributions with theoretical expectations for signal and background. However, for our purposes, let us define the following dimensionless quantity in the limit of on-shell W^+:

$$\lambda = \lambda_0 \frac{M_{[\bar{b}\ell]}^2 - m_b^2}{M_{[b\ell]}^2 - m_b^2 + M_{W^\pm}^2} = \lambda_0 \frac{2p_{\bar{b}} \cdot p_\ell}{2p_b \cdot p_\ell + M_{W^\pm}^2} = \lambda_0 \frac{2p_{\bar{b}} \cdot p_\ell}{2p_t \cdot p_\ell}. \quad (3)$$

From (1), the differential distribution of λ translates directly to the chiral coupling strengths. λ_0 is the normalisation which is a function of the masses. Given that $M_{H^\pm}$ needs to be known approximately for our analysis to be of much use, we can define λ_0 for instance as follows:

$$\lambda_0 = \frac{m_t^2 - M_{W^\pm}^2}{M_{H^\pm}^2 - m_t^2} \approx \frac{(2p_b \cdot p_\ell)_{\max}}{(2p_{\bar{b}} \cdot p_\ell)_{\max}}. \quad (4)$$

The dependence on λ observed will be the sum of the signal and the background which, after the signal selection cuts, is compatible with $H^\pm$ production. If the background does not involve chiral interactions, the distribution is flat, and even when the background does involve chiral interactions, the distribution can be analysed as the linear combination of the signal and background expectations. One can compare the ratio thus obtained with the signal to background ratio observed in order to confirm the presence of $H^\pm$ signal.

In the next chapter we study the exact definitions of λ for different final states.

4 Results

4.1 Leptonic decay with charge tagging

The simplest case is the leptonic decay of the top quark, with the charge tagging of both bottom jets and the lepton. This allows us to assign all momenta correctly. The size of the sample will be limited, since in addition to the leptonic branching ratio of the top quark, the rate is reduced further by the requirement of bottom quark charge tagging, the efficiency of which one might roughly estimate to be around $(10\%)^2 = 1\%$.

In figure 2a we show the differential distribution of λ at $M_{H^\pm} = 500$ GeV. As stated in the previous chapter, the distribution is flat for $\tan\beta = \sqrt{m_t/m_b} \approx 6.4$, and rapidly approaches the large and small $\tan\beta$ limits away from this central value. Let us concentrate on the two representative extreme values $\tan\beta = 1.5$ and 30, and the central value $\tan\beta = 6.417$ from here on.

The finite energy resolution of detectors can lead to a finite spread in the invariant mass distribution [9]. The binning in our distributions of $\Delta\lambda = 0.1$ are fairly broad, corresponding to roughly 0.1 times the energy scale considered. For the quantity $(2p_t \cdot p_\ell)$ in the denominator of (3), this corresponds to the energy spread of $0.1m_t \sim 15$ GeV. This is similar to the resolution obtainable at LHC [10].

The dependence on $M_{H^\pm}$ is studied at $\tan\beta = 1.5$ and $\tan\beta = 30$ in figure 2b. We see that the scale normalisation of (4) is satisfactory, and there is little residual dependence on $M_{H^\pm}$.

4.2 Leptonic decay without charge tagging

Once we drop the bottom quark charge tagging requirement, we need to consider a new definition of b and $\bar{b}$ in the procedure outlined above. It is possible that the signal selection procedure has already picked out one or the other of the two bottom jets as belonging to the decay of the top quark. If this is the case, the assignment is again trivial. From here on we assume that this is not the case.

If $M_{H^\pm} \gg m_t$ the procedure is straightforward, as $\bar{b}$ and the top quark decay products point back-to-back, even when we consider the boost from the production process. In this case $2p_b \cdot p_\ell \lesssim m_t^2 - M_W^2$ and $2p_{\bar{b}} \cdot p_\ell = \mathcal{O}(M_{H^\pm}^2)$ is much greater than the other dot product. The author has verified that the distributions look identical to figure 2a if we simply take $(2p_b \cdot p_\ell)$ to be the smaller of the two dot products.

For general $M_{H^\pm}$, particularly when $(M_{H^\pm}^2 - m_t^2) \sim (m_t^2 - M_{W^\pm}^2)$ at $M_{H^\pm} \sim 250$ GeV, the two dot products have similar distributions. In this case the charge tagging discussed above is an effective strategy. Here we proceed by summing over the two distributions corresponding to the 'right' and 'wrong' assignments of bottom quark jets.

The resulting distributions are shown in figure 3 for $M_{H^\pm} = 200$ GeV. This is already sufficiently below the contaminated region. Note that the normalisation is to two. Comparing with figure 2a we see that the region $\lambda < 1$ is similar in two distributions, but figure 3 has tails at $\lambda > 1$ where most of the wrong assignment lies.

This result indicates that the mis-assignment of bottom quarks, for example from production processes, is unlikely to have significant effect on our analysis, because of the different kinematic limits on the invariant masses.

We see that the flatness of the 'background' $\tan\beta = \sqrt{m_t/m_b}$ case is retained here.

4.3 Hadronic decay

If the top quark decays hadronically, the mass reconstruction allows one to assign b and $\bar{b}$ correctly to the two bottom quark jets. We assume that this has been done already in the signal selection process. We also assume that bottom quark jets are distinguishable from light quark jets. However, the ℓ and ν of equation (1) are now indistinguishable unless we tag the charges of light quark jets as well as the bottom quark jets.

Here we choose to proceed by defining ℓ to be the jet which minimises $p_b \cdot p_{\rm jet}$.

The result is shown in figure 4. The distribution is somewhat flatter than the distributions in the leptonic channel, figures 2 and 3, reflecting the difficulty with which the light quark jets can be assigned to the parent quarks. $M_{H^\pm} = 500$ GeV is adopted, but the distribution for different $M_{H^\pm}$ are found to be similar.

The problem of assigning the jets correctly can be seen in figure 5 which compares the differential distributions in invariant masses $M^2_{[bq]}$ and $M^2_{[b\bar{q}']}$. The distributions are roughly independent of either $M_{H^\pm}$ or $\tan\beta$. We see that the two dot products have similar profiles, and our procedure can not escape contamination from the wrong assignment.

4.4 The effect of cuts for the hadronic decay

The above discussions for the hadronic decay assume that the parton directions are known from the jet distributions. In practice, the jets can overlap when either top quark decay products being produced from relatively light $H^\pm$ interfere with the $\bar{b}$ jet, or when the top quark is boosted in heavy $H^\pm$ decay and the decay products are clustered near each other. These cases lead to ambiguous definitions of jet momenta.

Let us study the effect of jet showering by introducing cuts on jet separations.

A typical azimuthal-pseudorapidity separation $\Delta R = \sqrt{(\Delta\phi)^2 + (\Delta\eta)^2}$ required to define jets and reduce the inter-jet interference might be taken to be 0.7. In terms of the azimuthal angle at zero rapidity this corresponds to 0.7 radians, or 40 degrees.

Let us proceed by replacing ΔR by the angle between two jets in the rest frame of $H^\pm$.

We do not consider the effect of nonzero $H^\pm$ momenta. This is sensitive to the selection cuts imposed in order to reduce the background.

The ratio of events passing the cuts is shown in figure 6. The suppression is severe at large $M_{H^\pm}$ where the production cross section also falls. From the events which do pass the separation cuts, it is difficult to extract correlation effects. At $M_{H^\pm} = 1$ TeV, for example, the effects vanish altogether.

The distribution after cuts is shown in figures 7 for $M_{H^\pm} = 200$ GeV and 500 GeV, to be compared with figure 5 before cuts. The normalisations are to unity before cuts.

The effect of cuts is found to be significant, but not prohibitive in studying top quark polarisation.

4.5 Production processes

In order to study the effect of boosts on $H^\pm$ momenta from the production process, we consider the production process $gb \to tH^-$. The distributions are expected to be modified slightly because of the boosts on $H^\pm$ momenta acquired from the production. For the calculation of the production process we proceed as in [3].

In figures 8 we show distributions analogous to 7 for the hadronic decay after cuts. The cuts are now in terms of ΔR in the collider frame rather than the angle between jets. The normalisation is to unity after cuts for each distribution. We see that the distributions are not significantly affected by the boost.

The detector cuts on pseudorapidity, and any other separation cuts involving jets arising from the production process, for example the top quark in $gb \to tH^-$, can only affect the normalisation of the distribution. The separation cuts between the $H^\pm$ decay products are significant only because they directly affect the range of invariant masses accessible for our analysis.

For the sake of completeness, the author has run an analogous simulation for the leptonic top quark decay with the cuts $\Delta R > 0.7$ between the bottom quark jets and $\Delta R > 0.4$ between the lepton and the bottom quark jets. The effect has been found to be small, as expected.

5 Conclusion

In this paper we studied the effect on top quark polarisation of the chiral charged Higgs boson $H^\pm$ coupling to fermions. We discussed the optimum variables λ which can be adopted in both leptonic and hadronic decays of the top quark.

The variable λ we adopted assumes that $M_{H^\pm}$ is already approximately known by the time we apply this analysis, either by the observation of a peak in invariant mass of $t\bar{b}$, or by the analysis of $H^\pm$ decay to $\tau\nu$ as mentioned in [3].

For the leptonic decay of the top quark, λ can be defined such that the distributions have the desired features of a clear momentum correlation effect and flat distributions for the background. Charge tagging the bottom quark jets and the lepton helps when $M_{H^\pm} \sim 250$ GeV.

The correlation effect is significant both for large and small $M_{H^\pm}$.

For the hadronic decay of the top quark, the momentum correlation effects are less pronounced, but it is still strong enough to be used as a signal for $H^\pm$ production.

The distributions are affected significantly in the hadronic decay case by the requirement of jet separations. This is especially the case for heavy $H^\pm$.

The boost on $H^\pm$ from the production process is found to give only a small effect, in the case of $gb \to tH^-$ production mode. We expect our analysis to be general to all production modes, at LHC and beyond.

In conclusion, top quark polarisation is useful for confirming the presence of $H^\pm$ in a sample of final states containing $t\bar{b}$ in experimental analyses of near future, at $\tan\beta \gtrsim 9$ and $\tan\beta \lesssim 4$, and up to $M_{H^\pm} \sim 500$ in both hadronic and leptonic channels.

Acknowledgements

I thank Stefano Moretti for discussions, for pointing out reference [6] and for reading the manuscript. I also thank Kaoru Hagiwara and Mike Seymour for advice and discussions.

References

[1] F. Richard, *preprint* LAL 98–74, hep-ex/9810045, talk given at Zuoz Summer School on Hidden Symmetries and Higgs Phenomena, Zuoz, Switzerland, 16–22 August 1998.

[2] The ALEPH collaboration, *Phys. Lett.* **B429** (1998) 169.

[3] K. Odagiri, *preprint* RAL–TR–1999–012, hep-ph/9901432.

[4] A. Krause, T. Plehn, M. Spira and P.M. Zerwas, *Nucl. Phys.* **B519** (1988) 85;
V. Barger, R.J.N. Phillips and D.P. Roy, *Phys. Lett.* **B324** (1994) 236;
M. Guchait and D.P. Roy, *Phys. Rev.* **D55** (1997) 7263.

[5] B.K. Bullock, K. Hagiwara and A.D. Martin, *Phys. Rev. Lett.* **67** (1991) 3055.

[6] A. Czarnecki and J.L. Pinfold, *Phys. Lett.* **B328** (1994) 427.

[7] A. Mendez and A. Pomarol, *Phys. Lett.* **B252** (1990) 461, *ibidem* **B265** (1991) 177;
A. Djouadi and P. Gambino, *Phys. Rev.* **D51** (1995) 218.

[8] G.P. Lepage, *Jour. Comp. Phys.* **27**, (1978) 192.

[9] J.F. Gunion, *Phys. Lett.* **B322** (1994) 125.

[10] CMS Technical Proposal, CERN/LHC/94-43 LHCC/P1 (December 1994);
ATLAS Technical Proposal, CERN/LHC/94-43 LHCC/P2 (December 1994).

Figure captions

Figure 1: The tree level Feynman graph for the decay $H^+ \to t\bar{b}$ and subsequent top quark and W^+ boson decays. The H^- decay can be obtained trivially from H^+ decay.

Figure 2: The differential distribution of λ for the leptonic decay of the top quark, with charge tagging. Normalisation is to unity. Lines were used instead of histograms for the sake of clarity. The binning width is 0.1. (a – top) $M_{H^\pm} = 500$ GeV, for five different values of $\tan\beta$. (b – bottom) $\tan\beta = 1.5$ and $\tan\beta = 30$, for three different values of $M_{H^\pm}$. The $\tan\beta = 30$ distributions have negative gradients.

Figure 3: The differential distribution of λ for the leptonic decay of the top quark, without charge tagging. $M_{H^\pm} = 200$ GeV, for three different values of $\tan\beta$. Normalisation is to two.

Figure 4: The differential distribution of λ for the hadronic decay of the top quark, before cuts. $M_{H^\pm} = 500$ GeV, for three different values of $\tan\beta$.

Figure 5: The differential distribution of two invariant masses $M^2_{[bq]}$ and $M^2_{[b\bar{q}']}$, corresponding to 'b–nu' and 'b–lep' respectively in the figure legends, in the hadronic decay of the top quark. $M_{H^\pm} = 500$ GeV, $\tan\beta = 1.5$.

Figure 6: The ratio of $H^\pm$ decay events which pass the jet separation requirement, for three different values of $\tan\beta$ and 200 GeV $\leq M_{H^\pm} \leq 1$ TeV.

Figure 7: The differential distribution of λ for the hadronic decay of the top quark, after cuts. (a – top) $M_{H^\pm} = 200$ GeV; (b – bottom) $M_{H^\pm} = 500$ GeV. The normalisation is to unity before cuts.

Figure 8: The differential distribution of λ for the hadronic decay of the top quark, after cuts, convoluted with $g\bar{b} \to \bar{t}H^+$ production process. (a – top) $M_{H^\pm} = 200$ GeV; (b – bottom) $M_{H^\pm} = 500$ GeV. The normalisation is to unity after cuts.

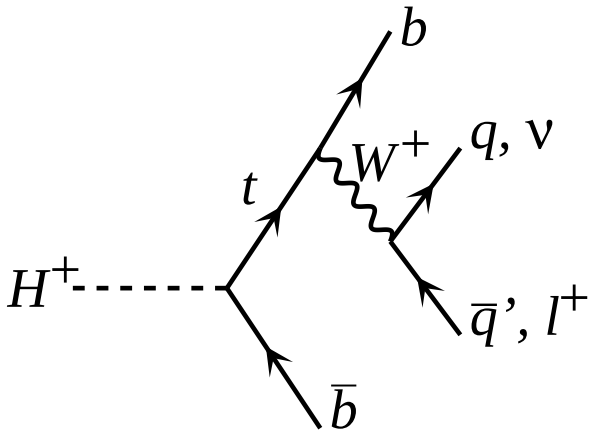

Figure 1

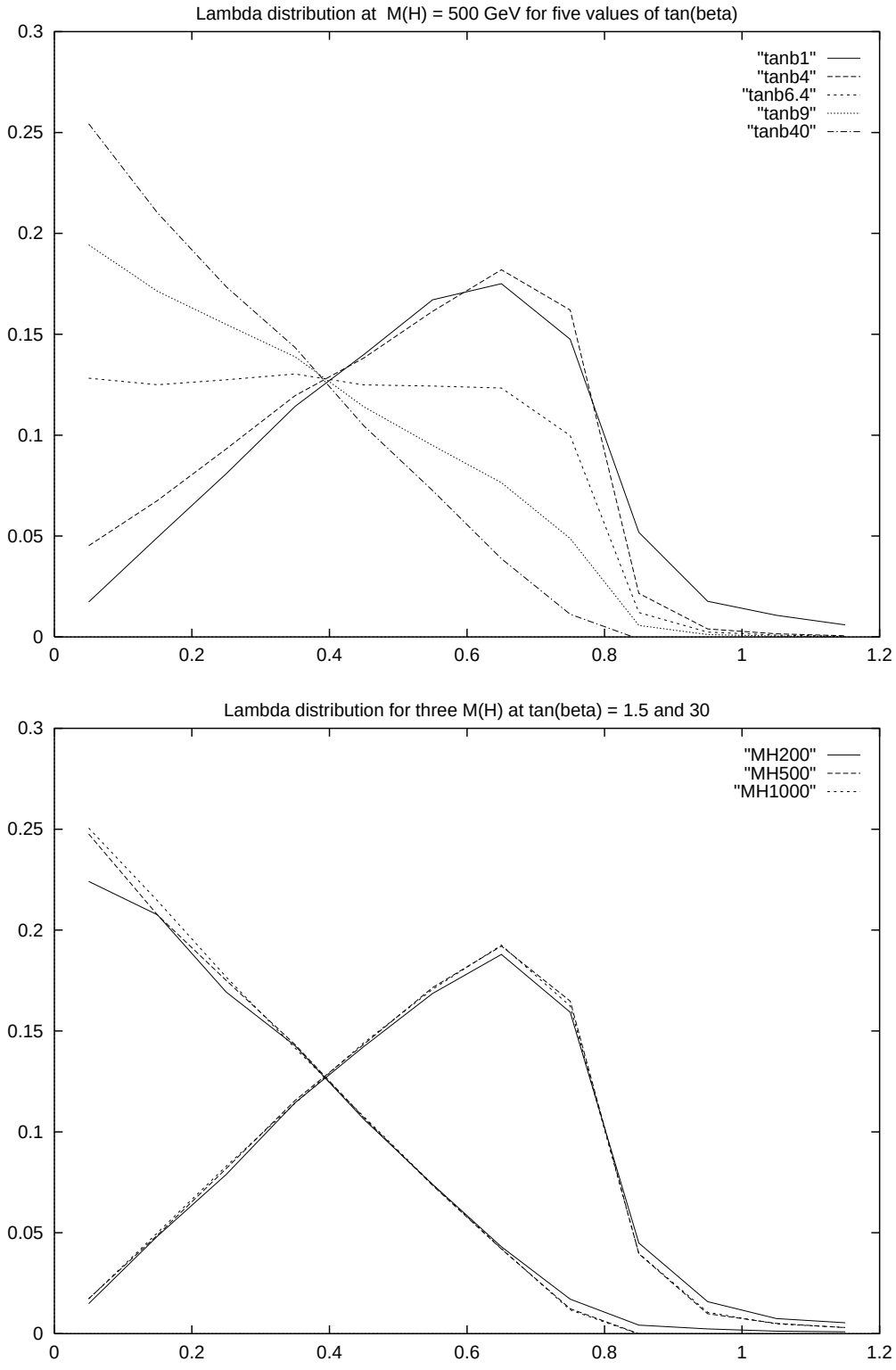
Lambda distribution at M(H) = 500 GeV for five values of tan(beta)
"tanb1"
"tanb4"
"tanb6.4"
"tanb9"
"tanb40"
0.3
0.25
0.2
0.15
0.1
0.05
0
0
0.2
0.4
0.6
0.8
1
1.2
Lambda distribution for three M(H) at tan(beta) = 1.5 and 30
"MH200"
"MH500"
"MH1000"
0.3
0.25
0.2
0.15
0.1
0.05
0
0
0.2
0.4
0.6
0.8
1
1.2

Figure 2

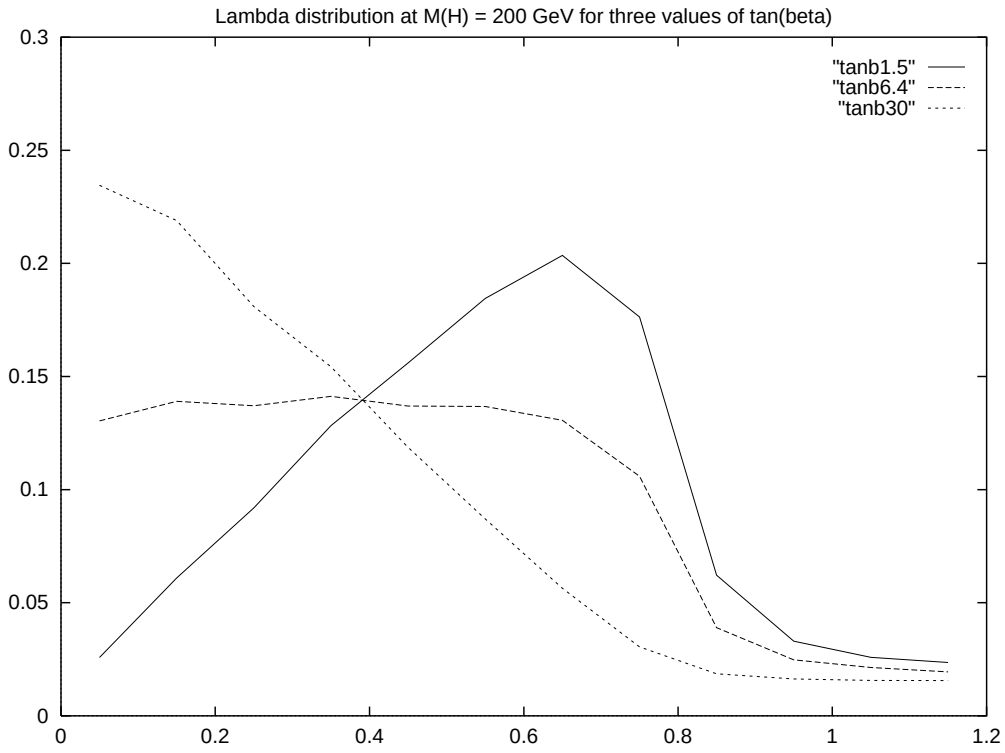
Lambda distribution at M(H) = 200 GeV for three values of tan(beta)
"tanb1.5"
"tanb6.4"
"tanb30"
0.3
0.25
0.2
0.15
0.1
0.05
0
0
0.2
0.4
0.6
0.8
1
1.2

Figure 3

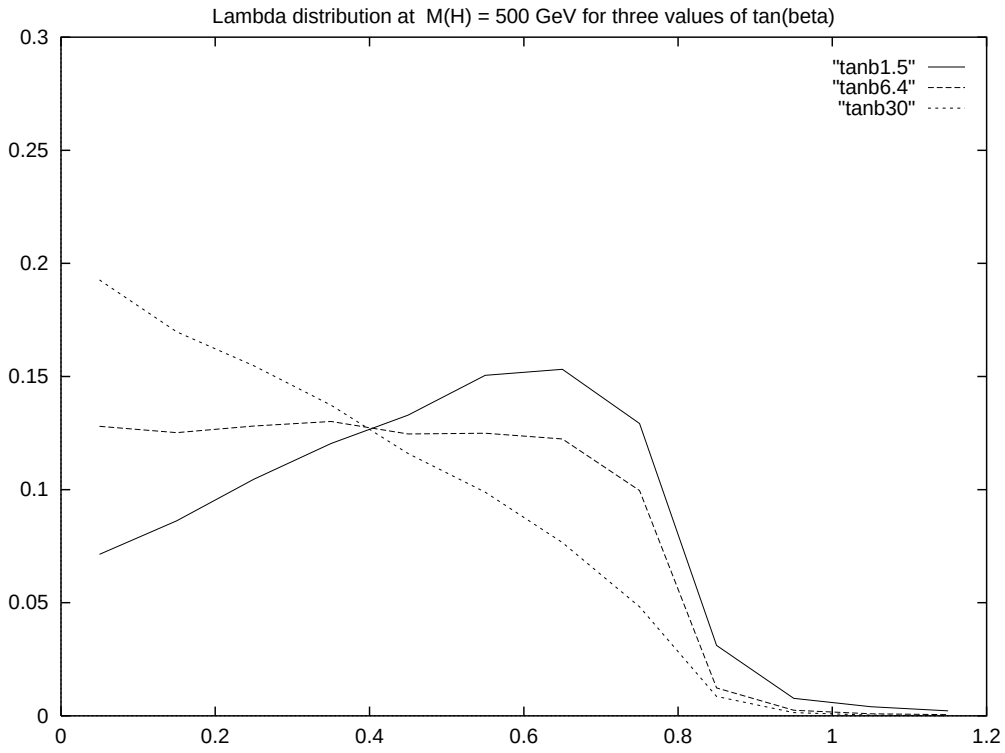
Lambda distribution at M(H) = 500 GeV for three values of tan(beta)
"tanb1.5"
"tanb6.4"
"tanb30"
0.3
0.25
0.2
0.15
0.1
0.05
0
0
0.2
0.4
0.6
0.8
1
1.2

Figure 4

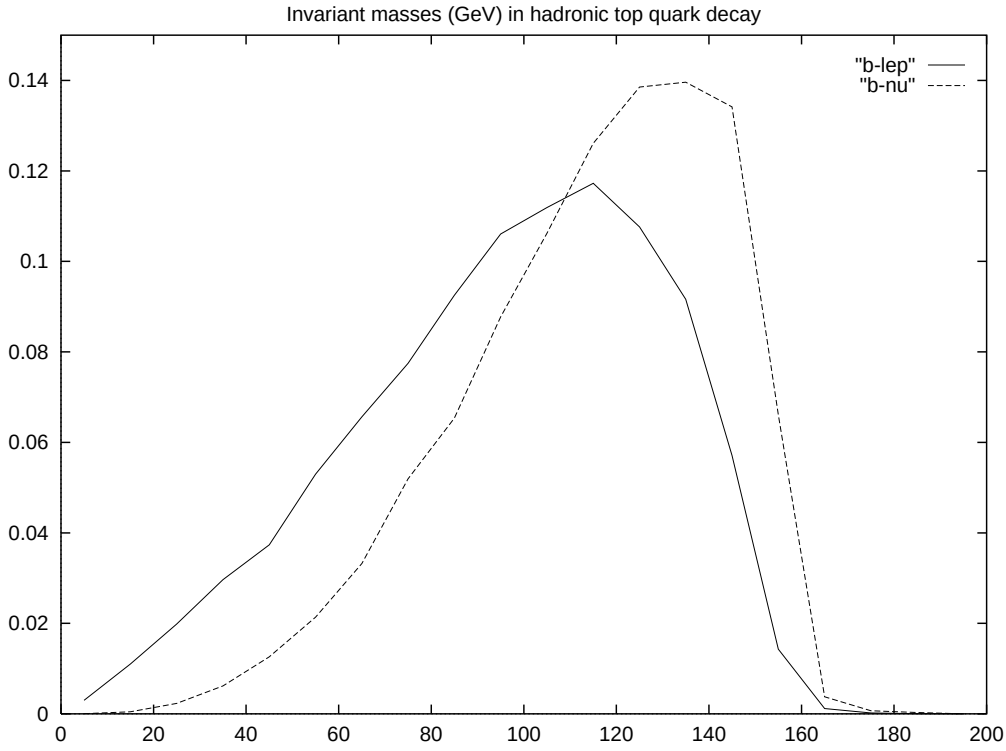
Invariant masses (GeV) in hadronic top quark decay
"b-lep"
"b-nu"
0.14
0.12
0.1
0.08
0.06
0.04
0.02
0
0
20
40
60
80
100
120
140
160
180
200

Figure 5

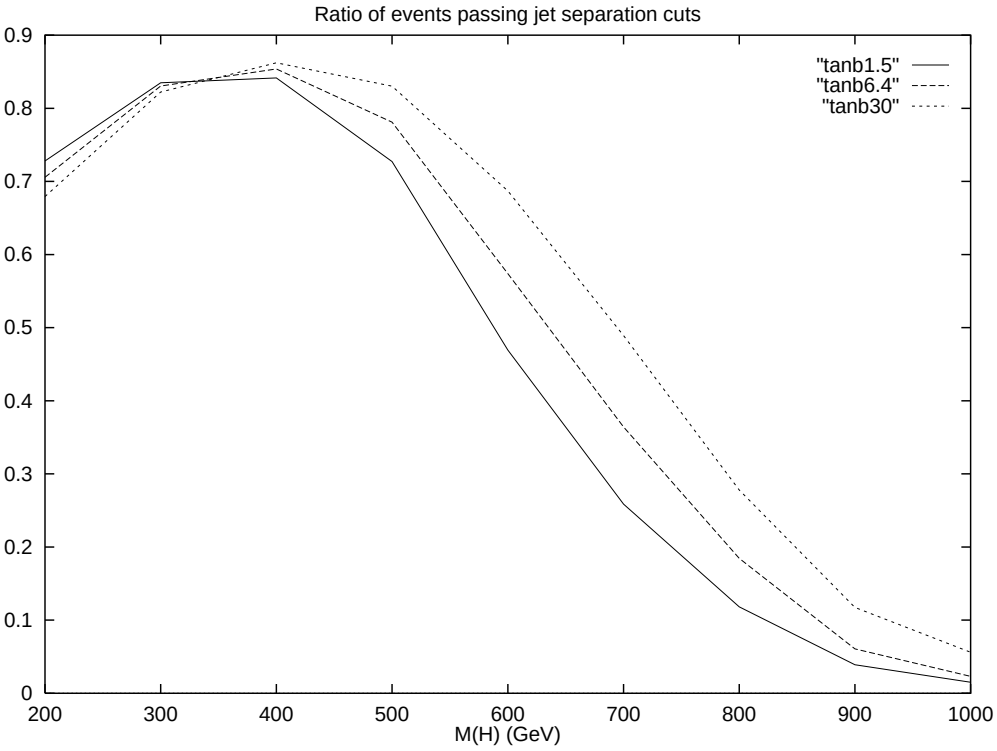
Ratio of events passing jet separation cuts
"tanb1.5"
"tanb6.4"
"tanb30"
0.9
0.8
0.7
0.6
0.5
0.4
0.3
0.2
0.1
0
200
300
400
500
600
700
800
900
1000
M(H) (GeV)

Figure 6

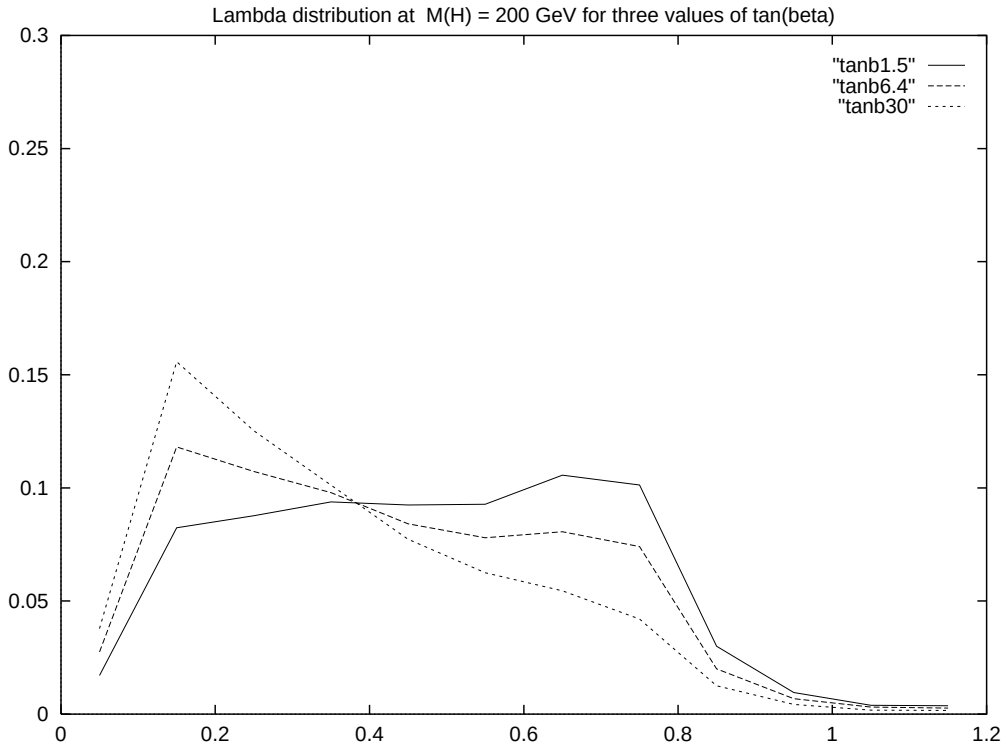
Lambda distribution at M(H) = 200 GeV for three values of tan(beta)
"tanb1.5"
"tanb6.4"
"tanb30"
0.3
0.25
0.2
0.15
0.1
0.05
0
0
0.2
0.4
0.6
0.8
1
1.2

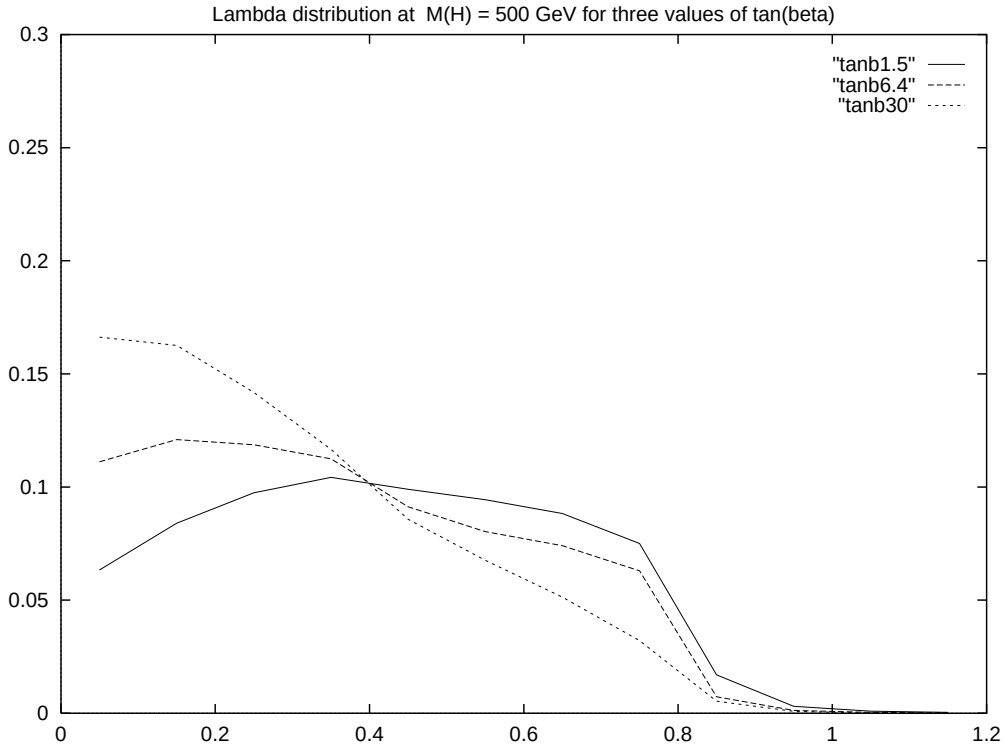
Lambda distribution at M(H) = 500 GeV for three values of tan(beta)
"tanb1.5"
"tanb6.4"
"tanb30"
0.3
0.25
0.2
0.15
0.1
0.05
0
0
0.2
0.4
0.6
0.8
1
1.2

Figure 7

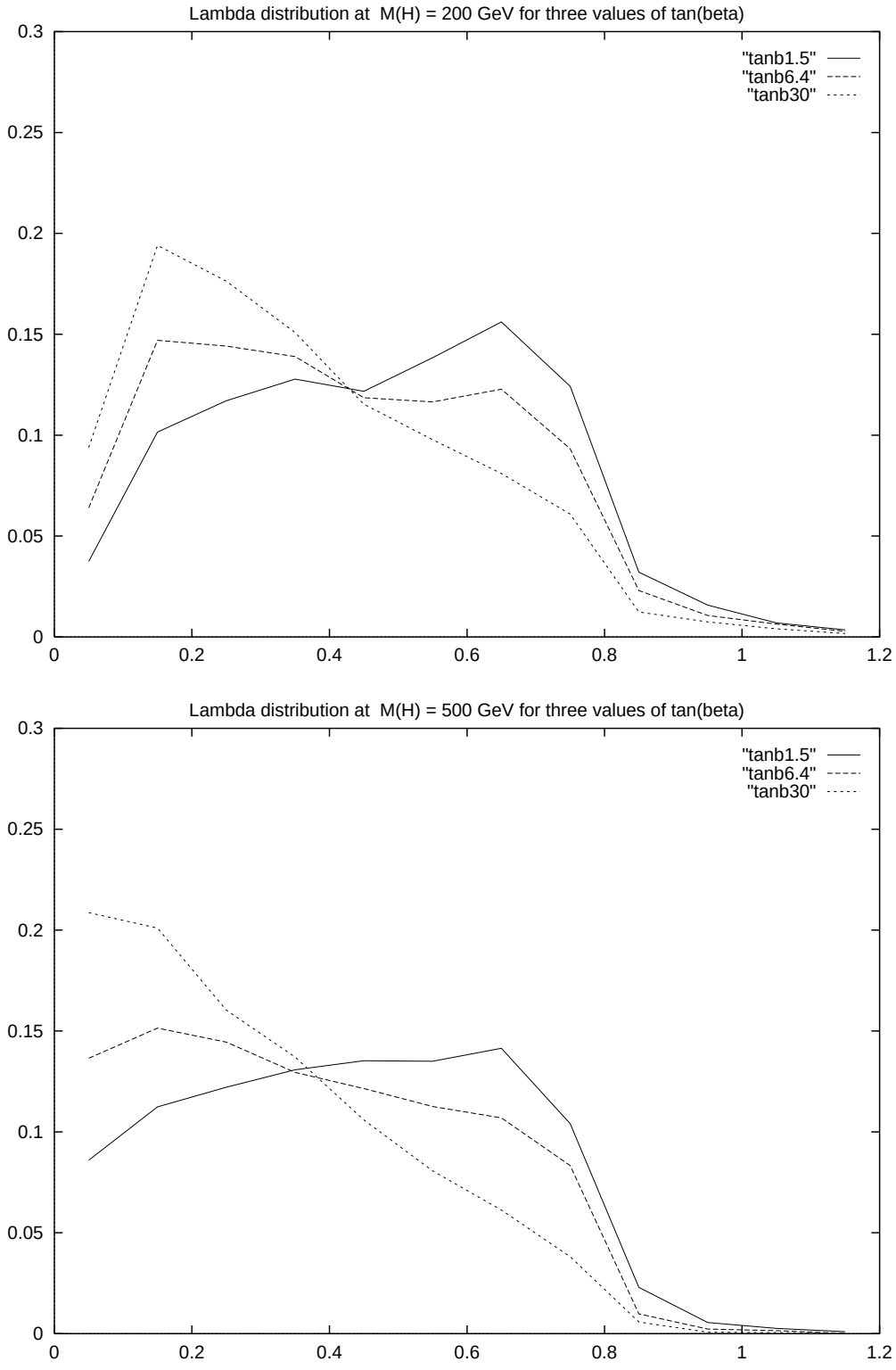
Lambda distribution at M(H) = 200 GeV for three values of tan(beta)
"tanb1.5"
"tanb6.4"
"tanb30"
0.3
0.25
0.2
0.15
0.1
0.05
0
0
0.2
0.4
0.6
0.8
1
1.2
Lambda distribution at M(H) = 500 GeV for three values of tan(beta)
"tanb1.5"
"tanb6.4"
"tanb30"
0.3
0.25
0.2
0.15
0.1
0.05
0
0
0.2
0.4
0.6
0.8
1
1.2

Figure 8